

Supporting Information

Client-scaffold interactions suppress aggregation of a client protein in model condensates

Rashik Ahmed^{1-4,*}, Rhea P. Hudson⁴, Julie D. Forman-Kay^{3,4}, and Lewis E. Kay^{1-4,*}

- 1) Department of Molecular Genetics, University of Toronto, Toronto, ON, Canada, M5S 1A8
- 2) Department of Chemistry, University of Toronto, Toronto, ON, Canada, M5S 3H6.
- 3) Department of Biochemistry, University of Toronto, Toronto, ON, Canada, M5S 1A8.
- 4) Program in Molecular Medicine, Hospital for Sick Children Research Institute, Toronto, ON, Canada, M5G 0A4.

*To whom correspondence should be addressed.

Keywords: NMR spectroscopy, phase separation, protein free-energy landscape, FUS RRM, CAPRIN1

Materials and Methods

Expression and purification of CAPRIN1, and RRM_s from FUS, TAF-15, and EWSR1

The C-terminal low-complexity disordered region of human CAPRIN1 comprising residues Ser607-Gln707 and containing the mutations N623T, N630T, V610A, L621A, referred to henceforth as CAPRIN1, was subcloned into a pET-His-SUMO vector. Substitution of Thr for Asn at positions 623 and 630 eliminates the formation of Iso-Asp linkages that would otherwise occur over time, as discussed previously(1), while removal of Val and Leu residues in the scaffold enables observation of methyl signals from spectra of the FUS RRM client without interference from peaks derived from CAPRIN1(2). *Escherichia coli* BL21 (DE3) RIPL cells were transformed with the vector bearing the CAPRIN1 sequence and grown to an OD₆₀₀ ~ 0.6 – 0.8. Protein expression was induced with 0.5 mM IPTG and allowed to continue overnight at 25 °C in LB (M9 minimal media) for unlabeled (isotopically labeled) protein. For production of 99.99% ¹⁴N CAPRIN1, cells were supplemented with 1 g/L 99.99% ¹⁴N-(NH₄)₂SO₄ (Sigma Aldrich) as the sole nitrogen source. Uniformly ¹³C-labeled CAPRIN1 was produced by supplementing M9 minimal media with 3 g/L D-Glucose-13C₆ (Cambridge Isotope Laboratories) as the sole carbon source. Cells were harvested via centrifugation, resuspended in lysis buffer (6 M guanidinium chloride, 50 mM Tris pH 8, 500 mM NaCl, 10 mM Imidazole), and sonicated for 15 minutes (2 s on, 2 s off). Lysed cells were spun down at 13,800 g for 1 hour, and the supernatant was loaded onto a Ni-NTA column (GE Healthcare) equilibrated with lysis buffer. The column was washed extensively with lysis buffer and CAPRIN1 was eluted with a solution of 50 mM Tris pH 8, 150 mM NaCl, 400 mM imidazole. The His-SUMO tag was cleaved with HisSUMO protease while exchanging against 50 mM Tris pH 8, 150 mM NaCl, 10 mM imidazole, 2 mM β-mercaptoethanol buffer at 4 °C. The cleaved protein was loaded onto a Ni-NTA column to remove the His-SUMO tag and HisSUMO protease, concentrated, and injected onto a Superdex75 (26/600) column equilibrated with 3 M guanidinium chloride, 50 mM Tris pH 8. The purified protein fractions were pooled and stored at -20 °C until use.

The human FUS RRM (D276-T370), TAF-15 RRM (D232-E323), and EWSR1 RRM (D353-S453) sequences all bearing an N-terminal diglycine (GG) were subcloned into pET-His-SUMO vectors and transformed into *Escherichia coli* BL21 (DE3) RIPL cells. The cells were grown to an OD₆₀₀ ~ 0.6-0.8, protein expression induced with 0.5 mM IPTG, and protein expression continued overnight at 18 °C in M9 D₂O (H₂O) media supplemented with 3 g/L d₇-glucose (glucose) for deuterated (non-deuterated) protein production. Uniform ¹⁵N isotopic labeling was achieved by the addition of 1 g/L ¹⁵N ammonium chloride to the M9 growth medium. Methyl labeling was achieved by the addition of 100 mg/L of 2-keto-3-methyl-d₃-3-d₁-4-¹³C-butyrate (for non-stereospecific labeling of Leu, Val-¹³CH₃/¹²CD₃) and 60 mg/L of 2-keto-3-d₂-4-¹³C-butyrate (for ¹³CH₃ labeling of Ileδ1) one hour prior to the induction of protein expression. Cells were harvested by centrifugation, resuspended in lysis buffer (50 mM Tris pH 8, 300 mM NaCl, and 20 mM Imidazole) supplemented with lysozyme, RNase A (Roche) and protease inhibitor cocktail tablets (Roche), and sonicated for 15 minutes (2 s on, 2 s off). Lysed cells were spun down at 13,800 g for 1 hour, and the supernatant was loaded onto a Ni-NTA column (GE Healthcare). After extensive washing with lysis buffer, the RRM_s were eluted with a buffer comprised of 50 mM Tris pH 8, 150 mM NaCl, and 400 mM Imidazole. The His-SUMO tag was cleaved with HisSUMO protease during constant buffer exchange with 50 mM Tris pH 8, 150 mM NaCl, 20 mM imidazole, 2 mM β-mercaptoethanol, 10% glycerol buffer at 4 °C. The cleaved protein was isolated through another round of Ni-NTA purification, concentrated, and loaded onto a Superdex75 (26/600) column equilibrated with 50 mM Tris pH 8. The pure protein-containing fractions were pooled and stored at 4 °C until use.

Preparation of FUS RRM:CAPRIN1 condensed phases

CAPRIN1 and FUS RRM were buffer-exchanged into a solution of 20 mM MES pH 6.0, 0.5 mM EDTA using a HiPrep 26,10 Desalting column. Concentrated stocks of FUS RRM (> 1 mM) and CAPRIN1 (> 8 mM) were mixed on ice and allowed to equilibrate for 30 minutes. Phase separation was induced through 10% dilution of the FUS RRM:CAPRIN1 mixture with 20 mM MES pH 6.0, 2 M NaCl, 0.5 mM EDTA, 100% D₂O, resulting in a final NaCl concentration of 200 mM and 10% D₂O. A portion of the phase-separated mixture was then transferred into a 3-mm NMR tube and stored at 4 °C until the phase-separated droplets coalesced into a homogeneous condensed phase and settled at the bottom of the tube. The dilute phase was subsequently decanted and replaced with more of the phase-separated mixture and allowed to undergo another cooling and droplet fusion cycle. This process was repeated until a sufficient condensed phase volume had formed that occupies the entirety of the NMR receiver coil with the dilute phase above, as shown in Fig. 3A. The phase-separated sample was allowed to equilibrate to the measurement temperature (25 or 40 °C) for ~8 hours prior to recording NMR experiments. After completion of condensed phase NMR measurements at each temperature, some of the dilute phase sitting above was decanted into a separate 3-mm NMR tube to generate the dilute phase samples used for measurements reported in Fig. 3. The labeling of the CAPRIN1 and FUS RRM components of the FUS RRM:CAPRIN1 condensate varied depending on the NMR experiment. The spectra shown in Fig. 3E and Fig. 4 (blue), for example, were measured using a condensate comprising ²H, ¹⁵N, ¹³C-ILV FUS RRM and ¹⁴N CAPRIN1 (¹⁴N at 99.7% abundance), while the samples prepared for the experiments shown in Fig. 4 (red) and Fig. 5 consisted of ²H, ¹⁵N FUS RRM and ¹⁴N CAPRIN1 (¹⁴N at 99.99% abundance) where one-third of the CAPRIN1 molecules were also uniformly ¹³C-labeled. Another phase-separated sample consisting of ¹⁵N, ¹³C FUS RRM and ¹⁴N CAPRIN1 (¹⁴N at 99.7% abundance) was prepared for assignment of FUS RRM resonances in the condensed phase and for monitoring its aggregation (Fig. 3I).

Circular dichroism (CD) thermal melts of RRM

CD thermal melts were performed on a Jasco J-1500 CD spectrometer using a 1 mm pathlength quartz cuvette. The CD signal at a wavelength of 218 nm was monitored over a temperature range of 30 °C to 80 °C, ramped at 1 °C per minute. RRM were prepared at 50 μM concentration either in 20 mM MES pH 6, 0.5 mM EDTA or 20 mM MES pH 5, 200 mM NaCl, 0.5 mM EDTA buffers. Spectra were smoothed with a first order Savitsky–Golay smoothing algorithm using a smoothing window of seven data points.

NMR measurements

NMR spectra were acquired on a 14.0-Tesla (600-MHz ¹H frequency) Bruker Avance III HD spectrometer, an 18.8 Tesla (800-MHz ¹H frequency) Bruker Avance III HD spectrometer, and a 23.5 Tesla (1 GHz ¹H frequency) Bruker Avance Neo spectrometer, all equipped with cryogenically cooled x, y, z pulsed-field gradient triple-resonance probes. An 11.7 Tesla (500-MHz ¹H frequency) Bruker Avance III HD spectrometer equipped with a liquid nitrogen-cooled z pulsed-field gradient triple-resonance probe was also used for monitoring RRM aggregation kinetics. Spectra were processed using NMRPipe(3) and analyzed with either NMRPipe, peakipy (<https://github.com/j-brady/peakipy>) or NMRFAM-SPARKY(4).

Assignment of FUS RRM folded and unfolded backbone amide resonances

Folded and unfolded FUS RRM backbone amide resonances were assigned using a suite of triple resonance 3D experiments, including 3D HNCO, HNCACO, HNCACB, HBCBCACONNH and HNN(5, 6), recorded using non-uniform sampling (NUS)(7) and processed with SMILE(8). Spectra were recorded at 40 °C on a mixed solution sample comprised of 0.9 mM ¹⁵N, ¹³C FUS RRM and 9 mM CAPRIN1 in 20 mM MES pH 6, 0.5 mM EDTA, 10% D₂O(5, 6). Under the conditions of these experiments approximately 30% of FUS RRM is unfolded.

Assignments were transferred to the condensed phase by recording 3D HNCO and HNCACO experiments after phase-separating the sample with the addition of NaCl to a final concentration of 200 mM, using the protocol described above.

1D ^{15}N -edited ^1H NMR spectra for monitoring aggregation of RRM (Fig. 1C-E)

A timeseries of one dimensional ^{15}N -edited ^1H NMR spectra were recorded to monitor the aggregation kinetics of 0.5 mM ^{15}N -labeled FUS, TAF-15 and EWSR1 RRM in the absence and presence of 4 mM CAPRIN1. A ‘dummy’ sample containing a lower concentration of the protein in buffer was first used to optimize acquisition parameters so that the acquisition could begin shortly after insertion of the ‘real’ sample into the magnet. Spectra were recorded under fully relaxed conditions, *i.e.*, using a recycle delay of 5 s, and either 160 or 320 scans for total acquisition times of 15 or 30 mins, as needed to sufficiently sample the aggregation kinetics. The integral over the entire amide envelope was measured to determine the amount of NMR-visible RRM. Note that the concentration of natural abundance ^{15}N -CAPRIN1 in the 4 mM CAPRIN1 samples is 12 μM so that the contribution from it to the measured integral can be neglected.

Concentration-dependent 3D HNCO peak intensity measurements for determining intermolecular FUS RRM interaction sites (Fig. 2)

Three-dimensional HNCO spectra were recorded at 45 °C on uniformly ^{15}N , ^{13}C -labeled FUS RRM prepared at 0.15 mM and 0.6 mM concentrations in 20 mM MES pH 6, 0.5 mM EDTA, 5% D_2O buffer. Spectra were recorded with two scans, a recycle delay of 1.5 s, 17% NUS, and ^{15}N and ^{13}C acquisition times of 50 and 35 ms, respectively, for net experimental measurement times of \sim 5 hours. Peak intensities in the two 3D HNCO datasets were determined using NMRFAM-SPARKY. Intermolecular interactions were quantified by monitoring the decrease in HNCO peak intensities in the high ($I_{\text{concentrated}}$) vs. low (I_{dilute}) concentration datasets, after adjusting for the 4-fold concentration difference between samples.

Measurement of water content in the dilute and condensed phases of phase-separated samples (Fig. 3B,D)

The concentration of water, both H_2O and D_2O , in the condensed and dilute phases was determined based on the integrals of the H_2O (D_2O) peak in ^1H (^2H) NMR spectra. Single-scan ^1H NMR spectra were recorded at 25 °C on an 800 MHz spectrometer using a one-pulse acquire scheme with a low receiver gain to prevent receiver overflow, and an acquisition time of 64 ms. ^1H pulses were centered on the water line, and a series of spectra were recorded with flip angles of {45°, 22.5°, 10°, 5°, 2.5°} and subsequently quantified. Similarly, single-scan ^2H NMR spectra were recorded at 25 °C on a 500 MHz spectrometer using an acquisition time of 100 ms with ^2H pulses centered on the water line. Comparison of H_2O and D_2O peak integrals in either the dilute or condensed phase samples with that of a reference buffer sample containing 90% H_2O and 10% D_2O was used to calculate the molar concentrations of water in each phase, as follows:

$$\left(\frac{V_{\text{H}_2\text{O},x}}{V_{\text{H}_2\text{O},\text{Ref}}} \right) x 0.9 x 55 \text{ M} + \left(\frac{V_{\text{D}_2\text{O},x}}{V_{\text{D}_2\text{O},\text{Ref}}} \right) x 0.1 x 55 \text{ M} \quad [\text{S1}]$$

where $V_{\text{H}_2\text{O},x}$ ($V_{\text{D}_2\text{O},x}$) is the integral of the H_2O (D_2O) peak in either the dilute or condensed phase and $V_{\text{H}_2\text{O},\text{Ref}}$ ($V_{\text{D}_2\text{O},\text{Ref}}$) is the integral of the H_2O (D_2O) peak in the reference sample. Note that concentrations of water calculated in this manner varied by less than 2 % as a function of ^1H pulse flip angle.

Measurement of the CAPRIN1 concentration in the FUS RRM:CAPRIN1 condensed phase via ^1H NMR (Fig. 3C,D)

The concentration of CAPRIN1 in the FUS RRM:CAPRIN1 condensed phase was determined by comparing peak integrals with a reference CAPRIN1 condensed phase sample of known concentration that lacks FUS RRM, as shown in Fig. 3C. Spectral regions from 1-2.1 ppm containing only proton peaks from CAPRIN1 were compared. Note that FUS RRM is deuterated with the exception of ILV methyl groups and backbone and sidechain amides; protons from methyls and amides resonate outside of the integrated region. Excitation-sculpting ^1H NMR spectra (9) were recorded at 25 °C on an 800 MHz spectrometer with an interscan delay of 5 s, 128 scans, and spectral width and acquisition times of 16 ppm and 64 ms, respectively. The condensed phase concentration of CAPRIN1 in the reference sample was determined through A_{280} measurements using an extinction coefficient of 10,430 M $^{-1}$ cm $^{-1}$. A 2 μL aliquot extracted directly from the condensed phase was diluted 100-fold with 8M guanidinium chloride to generate a well-dispersed solution amenable to absorbance measurements.

$[^1\text{H}, ^{13}\text{C}]$ methyl-TROSY ddHMQC NMR measurements of FUS RRM folded and unfolded populations and concentrations in CAPRIN1 dilute and condensed phases (Fig. 3F,G)

Methyl-TROSY spectra were recorded of dilute and condensed phase samples at 25 and 40 °C, 800 MHz, using a $[^1\text{H}, ^{13}\text{C}]$ ddHMQC pulse scheme with gradients for coherence transfer selection(2). Spectra were acquired under fully relaxed conditions with an interscan delay of 10 s, 8 scans/FID, ^{13}C spectral widths and acquisition times of 17 ppm and 25 ms, respectively, and a total acquisition time of 4 hours/spectrum. ^1H and ^{13}C pulses were centered on the water line and 19 ppm, respectively. Water suppression was obtained using coherence transfer selection gradients, with a water-selective EBURP1 pulse(10) (~ 7 ms) applied at the beginning of the scheme to ensure that the water signal is along the +Z axis at the start of ^1H acquisition.

Integrals of the eight dispersed folded isoleucine resonances and the overlapping unfolded cluster were measured and the fractional populations of the folded and unfolded states, P_F and P_U , respectively, were determined from the sum of the integrals of the folded and unfolded isoleucine resonances, accounting for differences in transverse relaxation of magnetization derived from the folded vs. unfolded species, as described previously(11):

$$P_F = \frac{\sum \frac{V_i^F}{\exp(-R_{2,eff,i}^F * t_{seq})}}{\sum \frac{V_i^F}{\exp(-R_{2,eff,i}^F * t_{seq})} + \sum \frac{V_T^U}{\exp(-R_{2,eff}^U * t_{seq})}} \quad [\text{S2}]$$

In Eq. [S2] V_i^F is the volume of “folded” (F) peak i , and V_T^U is the box-sum volume of the “unfolded” (U) peaks that cluster together, t_{seq} is the length of all fixed delays during the $[^1\text{H}, ^{13}\text{C}]$ ddHMQC experiment (4.6 ms), $R_{2,eff,i}^F$ is an effective ^1H single-quantum transverse relaxation rate for folded peak i , and $R_{2,eff}^U$ is the corresponding relaxation rate for the unfolded isoleucine cluster. Further details can be found in the SI Appendix of reference (11). The concentrations of the folded and unfolded FUS RRM species in the dilute and condensed phases were determined by comparing peak volumes with a FUS RRM sample in buffer of known concentration.

$1D$ $^{15}\text{N}(^{13}\text{C})$ -edited ^1H NMR spectra for monitoring aggregation of FUS RRM in buffer vs. dilute and condensed phases of FUS RRM:CAPRIN1 (Fig. 3I)

Condensed and dilute phase samples of FUS RRM:CAPRIN1 were prepared with $^{15}\text{N}, ^{13}\text{C}$ FUS RRM and ^{14}N CAPRIN1 (^{14}N at 99.7% abundance), using the protocol described above. Since the concentration of natural abundance ^{15}N CAPRIN1 in the condensed phase is ~90 μM , of the same order as the FUS RRM concentration (488 μM at 25 °C), 1D $^{15}\text{N}, ^{13}\text{C}$ -edited (HNCO-based) ^1H NMR spectra were recorded to selectively observe signals derived from FUS RRM. Integrals of the amide proton envelope in $^{15}\text{N}, ^{13}\text{C}$ -edited ^1H NMR spectra

recorded at 0 days vs. 89 days at 25 °C were compared to monitor the conversion of NMR visible FUS RRM protomers into NMR invisible aggregates. Measurements on the dilute phase sample were based on 1D ¹⁵N-edited ¹H NMR spectra (*i.e.*, without ¹³C editing) since the concentration of natural abundance ¹⁵N CAPRIN1 in the dilute phase is only ~8 μM and, therefore, signals from CAPRIN1 contribute negligibly to the measured integral. FUS aggregation kinetics in buffer were monitored using a 0.5 mM ¹⁵N,¹³C FUS RRM sample, approximately matching the condensed phase concentration of FUS RRM. As with the dilute phase, 1D ¹⁵N-edited ¹H NMR spectra were recorded at t=0 days and t=68 days for comparison.

2D ¹H-¹⁵N HSQC-based NOE experiment for mapping intermolecular FUS RRM:CAPRIN1 interactions in the condensed phase (Fig. 5)

A condensed phase sample of FUS RRM:CAPRIN1 was prepared with ²H, ¹⁵N FUS RRM and ¹⁴N CAPRIN1 (¹⁴N at 99.99% abundance) where one-third of the CAPRIN1 molecules were also uniformly ¹³C-labeled. Using the pulse scheme outlined in *SI Appendix*, *Fig. S2* and described previously(12), NOEs were recorded in the condensed phase to measure intermolecular contacts between protons coupled to ¹³C in the CAPRIN1 scaffold and protons coupled to ¹⁵N in FUS RRM client molecules. NOESY datasets were recorded using a gradient selected TROSY readout(13) with an interscan delay of 1.5 s, 128 scans/FID, NOE mixing time of 250 ms, and ¹⁵N $t_{1,max} = 50$ ms, for a total acquisition time of ~20 hours per experiment. A control experiment recorded on a ²H, ¹⁵N FUS RRM sample in buffer established that intra-molecular NOEs are not observed (*SI Appendix*, *Fig. S3*).

Table S1 – Thermodynamics of the folding – unfolding equilibrium of FUS RRM in dilute vs. condensed phases

Phase	25 °C							40 °C								
	P_F %	P_U %	[F] μM	[U] μM	[T] μM	K_p	$\Delta G_{F \rightarrow U}$ kJ/mol	$\Delta \Delta G_{F \rightarrow U}$ kJ/mol	P_F %	P_U %	[F] μM	[U] μM	[T] μM	K_p	$\Delta G_{F \rightarrow U}$ kJ/mol	$\Delta \Delta G_{F \rightarrow U}$ kJ/mol
Dilute	92.3	7.7	201	17	218	2.2	6.2	-4.2	74.6	25.4	155	53	208	2.5	2.8	-4.3
Condensed	69.2	30.8	338	150	488		2.0		36.4	63.6	192	335	527		-1.5	

$$\Delta \Delta G_{F \rightarrow U} = \Delta G_{F \rightarrow U}^{cond} - \Delta G_{F \rightarrow U}^{dil}$$

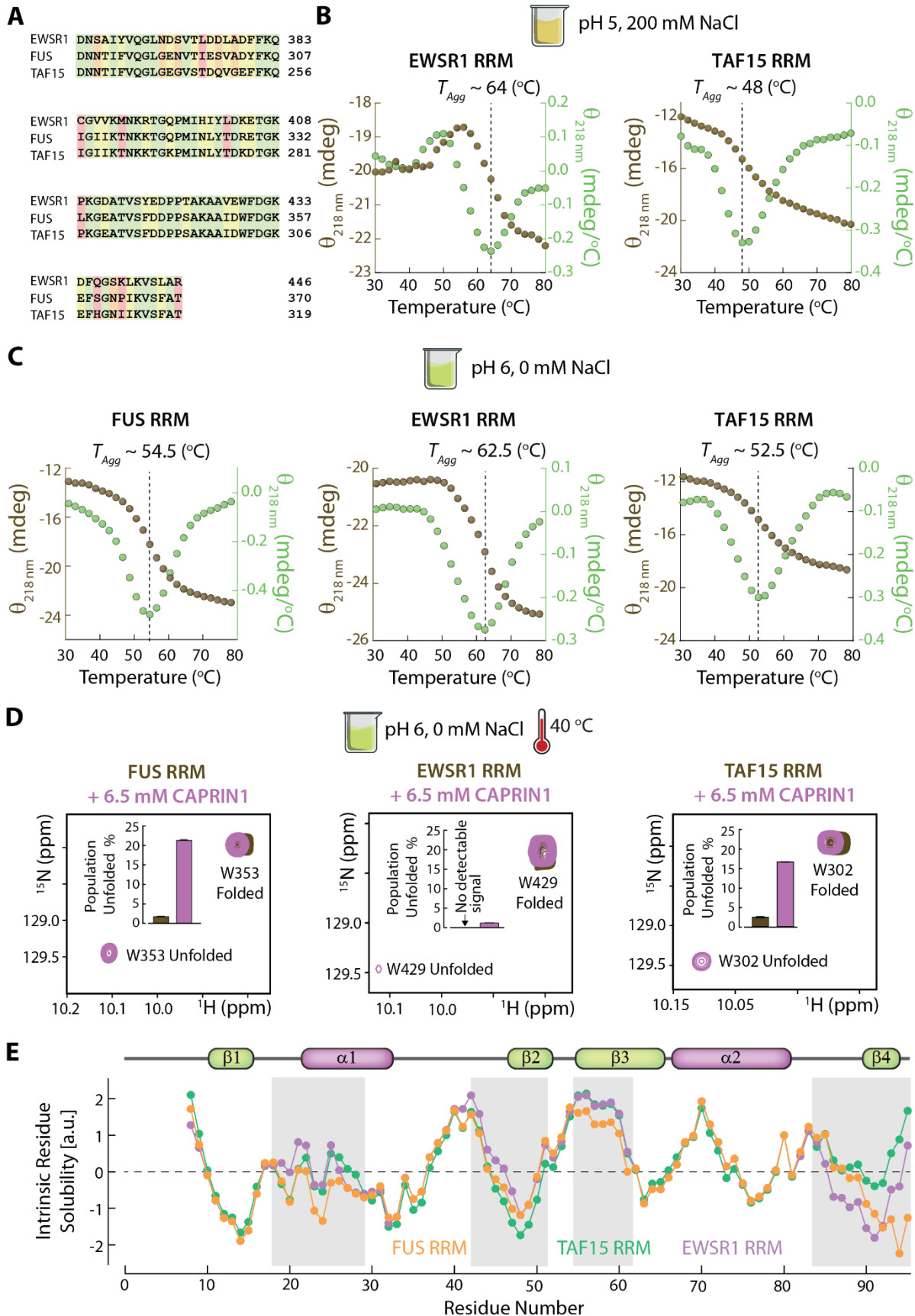


Figure S1 – Thermal melts, CAPRIN1-induced unfolding and predicted solubility of FUS, EWSR1, and TAF15 RRM. (A) Sequence alignments of FUS, EWSR1, and TAF15 RRM, with green highlighting identical residues in all sequences, yellow signifying amino acids with similar properties at a given position, orange denoting weaker similarity between residues at a given position, and red indicating no significant similarities between residues. (B) Circular dichroism (CD) thermal melts monitoring the β -sheet signature at 218 nm (brown) of EWSR1 RRM (left) and TAF15 RRM (right) in MES pH 5 buffer with 200 mM NaCl. The derivatives of the thermal melt profiles are shown in green. (C) As (B), except for FUS RRM (left), EWSR1 RRM (center), and TAF15 RRM (right) in MES pH 6 buffer with 0 mM NaCl. (D) Zoomed-in expansions of ^1H , ^{15}N TROSY-HSQC spectra of FUS (left), EWSR1 (center), and TAF15 (right) RRM in the absence (brown) and presence (purple) of 6.5 mM CAPRIN1 highlighting the tryptophan indole peaks derived from the folded and unfolded states of the RRM. Panel insets indicate the populations of the unfolded state, as determined from the peak volumes. (E) Predicted per-residue solubility of FUS (orange), TAF15 (green) and EWSR1 (purple) RRM, as per the CamSol method(14). Grey highlights indicate regions with large differences in solubility for the three RRM.

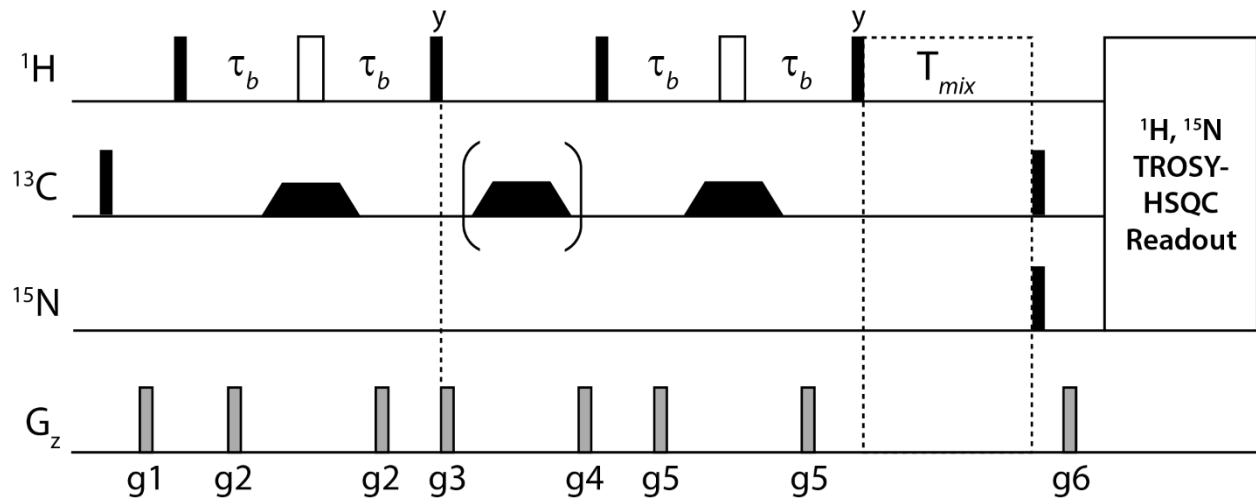


Figure S2 – 2D ^1H - ^{15}N based NOE pulse scheme for recording intermolecular NOEs connecting ^{13}C -bound protons of the CAPRIN1 scaffold and ^{15}N -bound protons of the FUS client (see above for labeling scheme). All rectangular ^1H and ^{13}C pulses are recorded at the highest possible power level, centered at the water frequency and at 67.5 ppm, respectively, while the ^{13}C trapezoidal-shaped adiabatic pulses(15) have broadband excitation profiles covering aliphatic and aromatic regions of the carbon spectrum (400 μs , 80 kHz sweep centered at 67.5 ppm, 11 kHz maximum B_1 field). The second adiabatic pulse (in parenthesis) is applied in alternate scans with concomitant inversion of the receiver phase. The value of τ_b is set to 1.7 ms, while a mixing time, T_{mix} , of 250 ms was used in the present set of experiments. The pulse sequence and parameters will be provided on Zenodo.

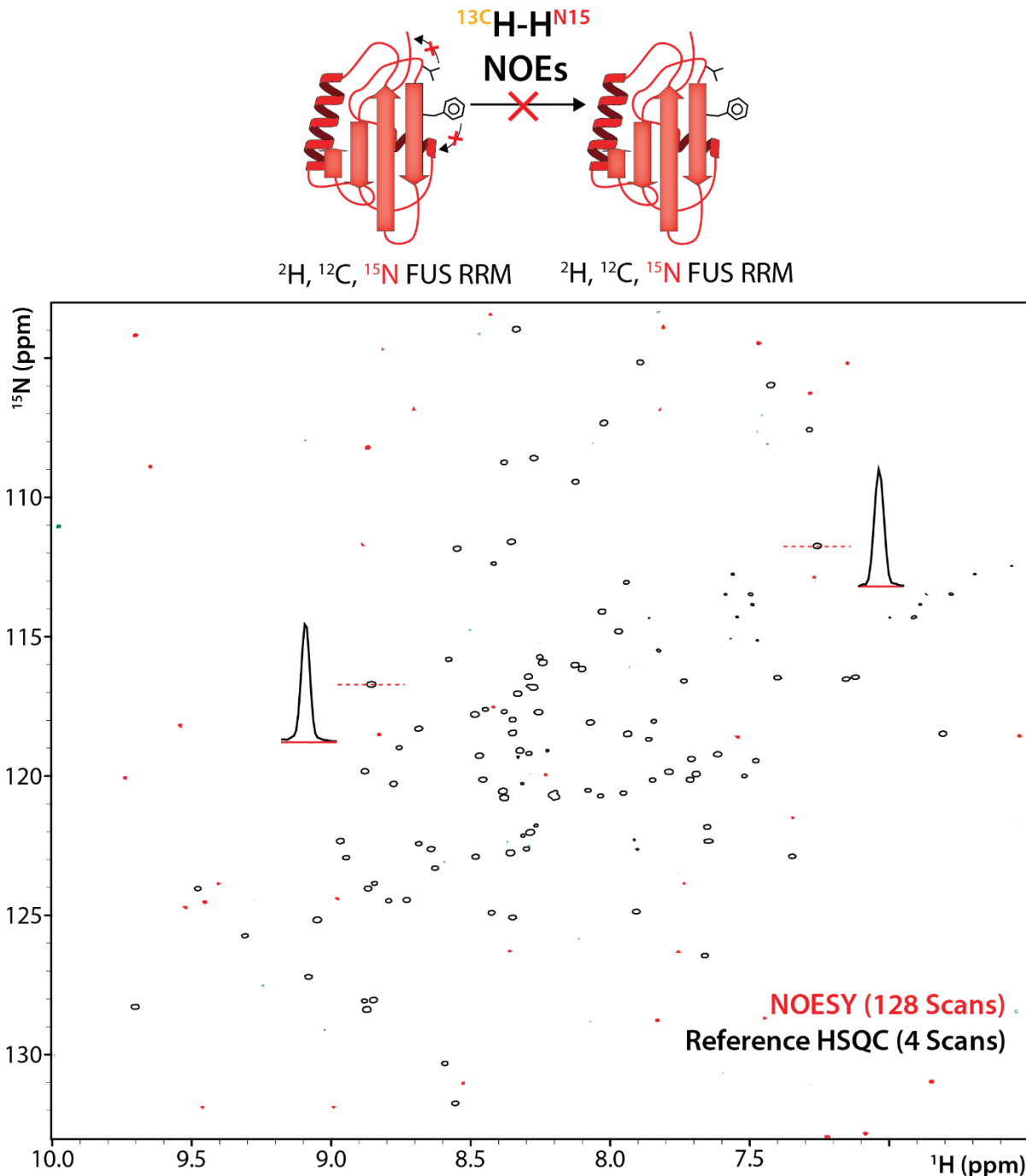


Figure S3 – NOESY control experiment. NOESY dataset (red) recorded using the scheme of Figure 2 with a mixing time of 250 ms at 1 GHz, 40 °C, is superimposed onto a reference $^1\text{H}, ^{15}\text{N}$ TROSY-HSQC spectrum (black, single contours). The NOESY experiment is recorded with 32-fold more scans than the HSQC. Several traces are shown, centered at positions of peaks in the HSQC spectrum (black). The absence of corresponding NOESY peaks indicates that intramolecular NOE correlations are not observed using the labeling scheme described above. Thus, the peaks in the NOESY spectrum of Figure 5b of the main text are not artifactual and derive from magnetization transfer from CAPRIN1 to FUS RRM.

References

1. Y. Toyama, A. K. Rangadurai, J. D. Forman-Kay, L. E. Kay, Mapping the per-residue surface electrostatic potential of CAPRIN1 along its phase-separation trajectory. *Proc Natl Acad Sci U S A* **119**, e2210492119 (2022).
2. R. Ahmed, *et al.*, A delayed decoupling methyl-TROSY pulse sequence for atomic resolution studies of folded proteins and RNAs in condensates. *J Magn Reson* **362**, 107667 (2024).
3. F. Delaglio, *et al.*, NMRPipe: A multidimensional spectral processing system based on UNIX pipes. *J Biomol NMR* **6**, 277–293 (1995).
4. W. Lee, M. Tonelli, J. L. Markley, NMRFAM-SPARKY: Enhanced software for biomolecular NMR spectroscopy. *Bioinformatics* **31**, 1325–1327 (2015).
5. M. Sattler, J. Schleucher, C. Griesinger, Heteronuclear multidimensional NMR experiments for the structure determination of proteins in solution employing pulsed field gradients. *Prog Nucl Magn Reson Spectrosc* **34**, 93–158 (1999).
6. S. C. Panchal, N. S. Bhavesh, R. V. Hosur, Improved 3D triple resonance experiments, HNN and HN(C)N, for HN and 15N sequential correlations in (13C, 15N) labeled proteins: application to unfolded proteins. *J Biomol NMR* **20**, 135–147 (2001).
7. S. G. Hyberts, D. P. Frueh, H. Arthanari, G. Wagner, FM reconstruction of non-uniformly sampled protein NMR data at higher dimensions and optimization by distillation. *J Biomol NMR* **45**, 283–294 (2009).
8. J. Ying, F. Delaglio, D. A. Torchia, A. Bax, Sparse multidimensional iterative lineshape-enhanced (SMILE) reconstruction of both non-uniformly sampled and conventional NMR data. *J Biomol NMR* **68**, 101–118 (2017).
9. T. L. Hwang, A. J. Shaka, Water Suppression That Works. Excitation Sculpting Using Arbitrary Wave-Forms and Pulsed-Field Gradients. *J Magn Reson A* **112**, 275–279 (1995).
10. H. Geen, R. Freeman, Band-selective radiofrequency pulses. *J Magn Reson* **93**, 93–141 (1991).
11. R. Ahmed, *et al.*, Atomic resolution map of the solvent interactions driving SOD1 unfolding in CAPRIN1 condensates. *Proc Natl Acad Sci USA* **121**, e2408554121 (2024).
12. T. H. Kim, *et al.*, Interaction hot spots for phase separation revealed by NMR studies of a CAPRIN1 condensed phase. *Proc Natl Acad Sci U S A* **118**, e2104897118 (2021).
13. J. P. Loria, M. Rance, A. G. Palmer, Transverse-Relaxation-Optimized (TROSY) Gradient-Enhanced Triple-Resonance NMR Spectroscopy. *J Magn Reson* **141**, 180–184 (1999).
14. P. Sormanni, F. A. Aprile, M. Vendruscolo, The CamSol Method of Rational Design of Protein Mutants with Enhanced Solubility. *J Mol Biol* **427**, 478–490 (2015).
15. J. M. Böhlen, G. Bodenhausen, Experimental Aspects of Chirp NMR Spectroscopy. *J Magn Reson A* **102**, 293–301 (1993).